

pubs.acs.org/JCTC Article

Capturing the Effects of Single Atom Substitutions on the Inhibition Efficiency of Glycogen Synthase Kinase-3 β Inhibitors via Markov State Modeling and Experiments

Ramin Mehrani, Jagannath Mondal, Davoud Ghazanfari, Douglas J. Goetz, Kelly D. McCall, Stephen C. Bergmeier, and Sumit Sharma*



Cite This: J. Chem. Theory Comput. 2024, 20, 6278-6286



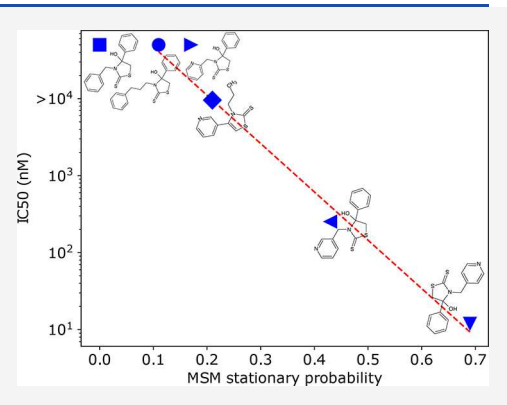
ACCESS I

III Metrics & More

Article Recommendations

Supporting Information

ABSTRACT: Small modifications in the chemical structure of ligands are known to dramatically change their ability to inhibit the activity of a protein. Unraveling the mechanisms that govern these dramatic changes requires scrutinizing the dynamics of protein—ligand binding and unbinding at the atomic level. As an exemplary case, we have studied Glycogen Synthase Kinase-3 β (GSK-3 β), a multifunctional kinase that has been implicated in a host of pathological processes. As such, there is a keen interest in identifying ligands that inhibit GSK-3 β activity. One family of compounds that are highly selective and potent inhibitors of GSK-3 β is exemplified by a molecule termed COB-187. COB-187 consists of a five-member heterocyclic ring with a thione at C₂, a pyridine substituted methyl at N₃, and a hydroxyl and phenyl at C₄. We have studied the inhibition of GSK-3 β by COB-187-related ligands that differ in a single heavy atom from each other (either in the location of nitrogen in their pyridine ring, or with the pyridine ring replaced by a



phenyl ring), or in the length of the alkyl group joining the pyridine and the N_3 . The inhibition experiments show a large range of half-maximal inhibitory concentration (IC_{50}) values from 10 nM to 10 μ M, implying that these ligands exhibit vastly different propensities to inhibit GSK-3 β . To explain these differences, we perform Markov State Modeling (MSM) using fully atomistic simulations. Our MSM results are in excellent agreement with the experiments in that they accurately capture differences in the binding propensities of the ligands. The simulations show that the binding propensities are related to the ligands' ability to attain a compact conformation where their two aromatic rings are spatially close. We rationalize this result by sampling numerous binding and unbinding events via funnel metadynamics simulations, which show that indeed while approaching the bound state, the ligands prefer to be in their compact conformation. We find that the presence of nitrogen in the aromatic ring increases the probability of attaining the compact conformation. Protein–ligand binding is understood to be dictated by the energetics of interactions and entropic factors, like the release of bound water from the binding pockets. This work shows that changes in the conformational distribution of ligands due to atom-level modifications in the structure play an important role in protein–ligand binding.

1. INTRODUCTION

Computational drug discovery has allowed researchers to rapidly screen vast libraries of compounds for potential drug candidates. Despite their many successes, high-throughput computational screening techniques are not accurate enough to predict the protein binding propensity of ligands that differ only slightly in their chemical structure. This is a critical stumbling block because even minor changes in the structure of ligands can significantly alter their binding affinity to a protein target. Therefore, after identifying potential drug scaffolds through computational screening, one has to undergo the painstaking process of trial-and-error optimization to produce a lead molecule. A way forward is to employ fully atomistic simulations coupled with methods that allow access to long time scales to capture the effects of subtle chemical changes on ligands' binding affinities. Markov State modeling (MSM) is one such approach wherein numerous unbiased

molecular dynamics (MD) trajectories are stitched to identify kinetically relevant states and rates of interconversion between them.^{2–5} MSM has been successfully employed to capture the dynamics of protein—ligand binding and unbinding events.^{6–13} Protein—ligand recognition is understood to occur via two prominent mechanisms: conformational selection, where a ligand binds to a pre-existing protein conformation, and induced fitting, where ligand binding induces a conformational change in the protein.^{7,8,10,14} However, these two mechanisms

Received: March 10, 2024 Revised: June 24, 2024 Accepted: June 26, 2024 Published: July 8, 2024





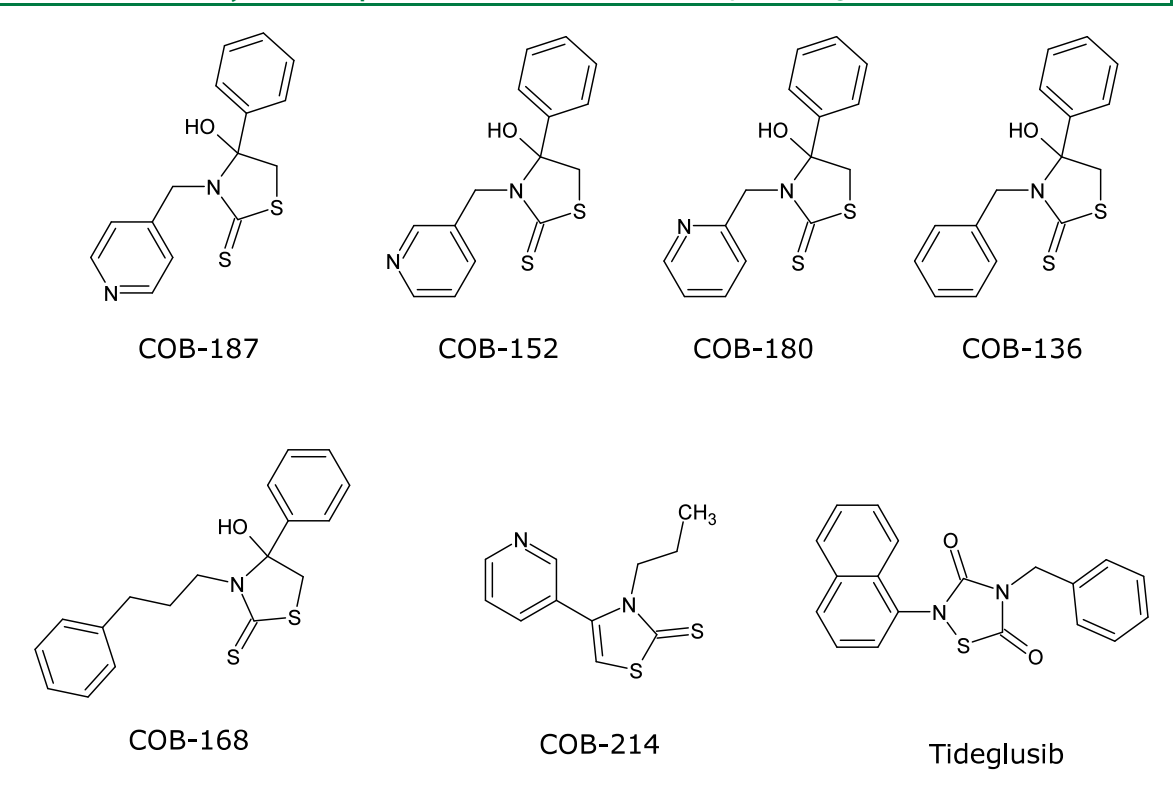


Figure 1. Seven different ligand molecules in close chemical space including COB-187: a five-member ring connected to a phenyl and a *p*-pyridine ring are studied. COB-152 and COB-180 differ from COB-187 in the location of the nitrogen atom in the pyridine ring. In COB-136, pyridine is replaced by a phenyl group. COB-168 has a longer alkyl group connecting the five-member ring to the aromatic ring. COB-214 is a slightly different structure with no −OH group connected to the five-member ring and pyridine group linked to the five-member ring from the carbon atom while the nitrogen in the five-member ring is connected to a propyl group, and Tideglusib.

by themselves do not explain why atom-level changes in the chemical structure of ligands can dramatically affect their binding propensity. The focus of this work is to accurately distinguish the binding propensities of closely related ligands on the ATP binding site of Glycogen Synthase Kinase-3 β (GSK-3 β) protein, using fully atomistic simulations and specialized modeling methodologies. Binding propensity of ligands onto proteins is often explained in terms of energetics of interactions and entropic effects, like the release of bound water from a protein's binding pockets. ^{15,16} We demonstrate that the conformational diversity of ligands, which is affected by atom-level differences, also plays an important role in their binding propensity.

GSK-3 is a serine/threonine kinase present in all eukaryotes that is involved in a multitude of signaling pathways. 17-20 GSK-3 exists in two isoforms [GSK-3 α (51 kDa) and GSK-3 β (47 kDa)]²¹ that exhibit 68% amino acid similarity. Beginning with its discovery as a kinase that regulates glucose metabolism in skeletal muscle, ²² GSK-3 is now associated with more than 40 different substrates. 23 Not surprisingly, abnormal activity of GSK-3 has been implicated in many diseases including cancer, metabolic disorders, and neurodegenerative diseases, thus making it an important therapeutic target.^{24–28} As such, there has been a vigorous effort to develop reagents that modify GSK-3 activity into therapeutics. Many reagents, predominantly small molecules, have been identified as GSK-3 inhibitors.^{29,30} Interestingly, lithium, which is currently used in the clinic, is a weak GSK-3 inhibitor.³¹ Besides this nonspecific and weak GSK-3 inhibitor, to date, no specific potent GSK-3 inhibitor has made it to market.³⁰ Tideglusib, arguably the most well-studied GSK-3 inhibitor, acts as an

irreversible non-ATP competitive inhibitor.³² While initially touted to be a specific GSK-3 inhibitor, 33 subsequent studies have shown that it acts on multiple kinases in addition to GSK-3.^{28,32} Tideglusib is currently undergoing Phase II clinical trials, and no other inhibitor has advanced beyond Phase II clinical trials.³⁴ The majority of GSK-3 inhibitors are ATPcompetitive inhibitors (e.g., AR-A014418).35 However, ATPcompetitive inhibitors are often promiscuous since nearly all kinases bind ATP and thus a compound that inhibits the binding of ATP to one kinase will likely inhibit ATP binding to multiple other kinases. Since there are over 500 kinases in the human genome, the potential for off-target kinase effects is quite substantial. That said, and somewhat in contrast to this logic, a more recently developed ATP-competitive inhibitor, 9-ING-41, is quite specific for GSK-3 and is in Phase II clinical trials. 36,37 Thus, there appears to be regions of the ATP binding site of GSK-3 that are unique among kinases.

Recently, we reported a set of novel GSK-3 inhibitors, exemplified by a compound termed COB-187, which are highly selective and potent inhibitors of both isoforms of GSK-3. ^{28,38} COB-187 appears to inhibit GSK-3 through a reversible and Cysteine (Cys)-199-dependent mechanism. ³⁸ It has been reported that GSK-3 activity is elevated in a dysfunctional innate immune response termed "cytokine storm" which can be attenuated by GSK-3 inhibitors. ³⁹ We previously investigated the ability of COB-187 to inhibit LPS (a component of Gram-negative bacteria) induced cytokine production and SARS-CoV-2 spike protein-induced CXCL10 (a chemokine elevated in patients with severe COVID-19) ⁴⁰ production. We found that COB-187 inhibited, at the protein and transcription level, nearly all of the cytokines induced by LPS, ⁴¹ and

dramatically inhibited SARS-CoV-2 spike protein induction of CXCL10. 42,43 Thus, COB-187 and related compounds hold significant promise as the basis for a new generation of highly selective GSK-3 inhibitors.

Interestingly, the discovery of this new set of compounds as GSK-3 inhibitors was largely serendipitous. As such, a detailed understanding of how this group of compounds interacts with GSK-3 is limited. Thus, key questions remain unanswered, such as: (i) Are there better inhibitors in the nearby chemical space? (ii) What is a rational approach for identifying such inhibitors? To begin to address these issues, it is imperative that the underlying molecular mechanisms responsible for the strong binding of COB-187-like molecules to GSK-3 be elucidated. Thus, in this study, we have employed Markov State Modeling (MSM) in molecular dynamics simulations to determine the binding affinity of a strategically selected set of small molecules (ligands) in the chemical space around COB-187 for the ATP-binding site of GSK-3 β . Note that our previous study suggested that COB-187 is an ATP-competitive inhibitor.³⁸ COB-187 consists of a five-member heterocyclic ring with a thione at C2, a pyridine substituted methyl at N3, and a hydroxyl and phenyl at C₄.

In this work, we have studied the inhibition of GSK-3 β by COB-187-related ligands that differ in a single heavy atom from each other (either in the location of nitrogen in their pyridine ring, or with the pyridine ring replaced by a phenyl ring), or in the length of the alkyl group joining the pyridine ring and N₃. We correlate the MSM results to molecular-level experimental data that characterize the potency of each ligand for GSK-3 inhibition. Our MSM results are in excellent agreement with the experimental data in that they accurately capture differences in the binding propensity of the ligands. The simulations reveal that the binding propensity of the ligands is related to their ability to attain a compact conformation. To verify this finding, we simulate numerous binding and unbinding events using funnel metadynamics simulations, which confirm that the ligands prefer a compact conformation while entering the bound state. The compact conformation of ligands is facilitated by the presence of a nitrogen atom in the aromatic ring.

2. METHODS

2.1. Simulation Details. We have studied the binding propensity of seven different ligands on the ATP binding site of GSK-3 β . As shown in Figure 1, these compounds are as follows: (1) COB-187: a five-member ring connected to a phenyl and a p-pyridine ring. (2) COB-152: similar to COB-187 with *m*-pyridine instead of *p*-pyridine. (3) COB-180: similar to COB-187 except for o-pyridine instead of p-pyridine. (4) COB-136: similar to COB-187 with a phenyl ring instead of the pyridine ring; that is, the nitrogen atom is replaced by a carbon atom in the ring. (5) COB-168: similar to COB-136 but has two more methylenes in the alkyl group that connects the five-member ring to the aromatic ring. (6) COB-214: a slightly different structure compared to the other four molecules with no OH group connected to the 5-member ring and m-pyridine linked to the 5-member ring from the carbon atom while the nitrogen in the 5-member ring is connected to a propyl group. (7) Tideglusib.

The crystal structure of GSK-3 β is taken from the Research Collaboratory for Structural Bioinformatics (RCSB) protein data bank, PDB (PDB ID: 1109), and missing residues are replaced using modeler. ⁴⁴ A GSK-3 β protein chain is solvated

with TIP3P water⁴⁵ and chloride ions are added to make the system charge-neutral. A ligand molecule is inserted at a random location in the simulation box so that it is at least 6 Å from the nearest protein atom. All simulations are performed using the Assisted Model Building with Energy Refinement (AMBER) molecular simulation package 46,47 using the ff14SB force field.⁴⁸ After building the simulation system, a two-step energy minimization is performed to remove any overlaps and for relaxing the configuration. In the first step, solvent molecules are energy minimized for 10,000 steps while keeping the protein structure restrained. In the second step, the restraints on the protein are removed and the whole system is energy minimized for 40,000 steps. Then the simulation system is heated to 310 K in 100 fs while maintaining the pressure at 1 bar using the Nosé-Hoover barostat. This is followed by a 100 ns isothermal-isobaric (constant number of particles, N, pressure, P, and temperature, T) simulation with the configurations saved every 0.1 ns. MSM requires a large number of equilibrated protein-ligand configurations. Therefore, the above steps are repeated to perform 200 independent simulations for each ligand molecule.

The first step to build a Markov State model^{2,3} is to perform a geometry-based clustering of configurations to generate microstates. To identify geometrically close configurations, we determine the distance between the heavy atoms of the ligand and the amino acid residues and convert the distance matrix into a contact map by setting the distance less than 5 Å to 1 and rest to 0. The VAMP2 score of this feature selection approach is higher than other approaches where we set the threshold distance at 8 Å or consider the minimum distance between the heavy atoms of the ligand and the amino acid residues (Figure S1, Supporting Information). Following this, we use Time-lagged Independent Component Analysis (TICA) to reduce the dimensionality of the feature matrix.^{49–52} TICA identifies the slow dynamical modes of the system by finding projections in the data that minimize the loss of kinetic information by maximizing the autocorrelation function for a specified lag time. TICA is analogous to performing principal component analysis in the dynamical space and provides rank-ordered eigenvectors. The MD configurations are classified into different microstates. By tracking transitions between the different microstates, we develop transition matrices associated with a range of lag times. The appropriate relaxation time of the underlying Markov process is identified using the implied time scale plot, which is a plot of relaxation time scales for different lag times. Figure S2 (Supporting Information) shows the implied time scale plots of each ligand. We classify the microstates into the MSM macrostates using the Perron Cluster Analysis (PCCA+).53 To ensure that the final model is Markovian, we evaluate the models using the Chapman-Kolmogorov test⁵⁴ (Figures S4-S10, Supporting Information). For each ligand molecule, we recover multiple macrostates associated with different binding sites on GSK-3 β and the stationary probabilities of each macrostate. The TICA lag time, TICA accuracy, number of microstates, MSM relaxation times, and the number of macrostates for each ligand are listed in Table S1 (Supporting Information). The MSM analyses are performed using the pyEMMA package⁵⁵ (http://pyemma.org).

2.2. Experimental Methods. GSK-3 kinase Z'LYTE assays are performed via contract research with Life Technologies/Thermo Fisher Scientific (Waltham, MA) as described.²⁸ This end-point assay measures the level of

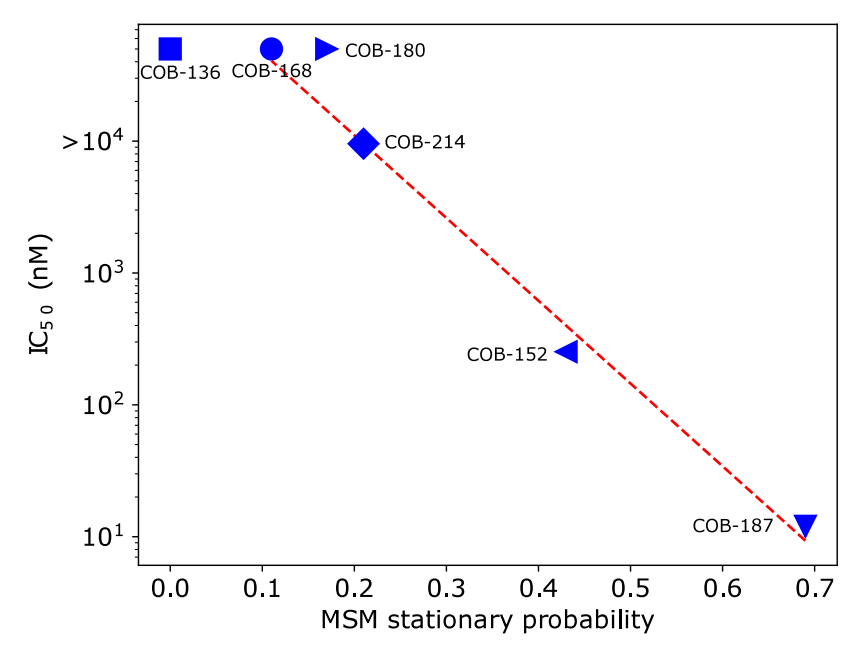


Figure 2. Comparison between the experimental IC_{50} values and MSM stationary probabilities of the ATP bound state of 6 ligand molecules. (square) COB-136, (circle) COB-168, (right triangle) COB-180, (tilted square) COB-214, (left triangle) COB-152, and (down triangle) COB-187. Tideglusib is not included because it does not show any binding to the ATP binding site in the simulations.

phosphorylation of the substrate, namely, human glycogen synthase I peptide, containing Ser641. Ten μ M ATP, 2 μ M substrate, 1.078 nM GSK-3 α or 0.753 nM GSK-3 β , and a test compound are mixed in 384-well plates and incubated at room temperature for 1 h. For COB-187, COB-152, and COB-214, the percent inhibition for a range of compound concentrations is determined and a plot of percent inhibition versus compound concentration is used to estimate the half-maximal inhibitory concentration (IC₅₀) of each compound. For COB-136 and COB-168, the percent inhibition is determined at a compound concentration of 10 μ M.

3. RESULTS AND DISCUSSION

Figure 2 shows a plot of IC_{50} values and stationary probabilities associated with the ATP-bound state of the six ligands studied by us (Tideglusib does not bind to the ATP

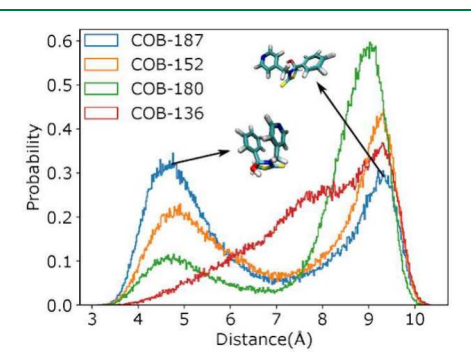


Figure 3. Probability distributions of the distance between the para atoms of the two six-member aromatic rings in COB-187, COB-152, COB-180, and COB-136. The para position is the fourth atom in the ring counting from the carbon that is attached to the rest of the molecule. COB-214 is structurally different with only a single six-member aromatic ring. COB-168 has a longer alkyl group than other molecules do. Figure S3 (Supporting Information) includes the distributions of COB-214 and COB-168.

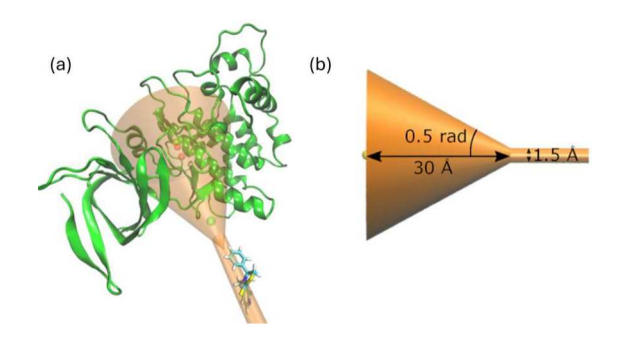


Figure 4. Funnel metadynamics setup: (a) location and orientation of the funnel region with respect to the GSK-3 β protein; (b) geometry of the funnel-shaped region.

binding site). IC_{50} is a widely used measure of a drug's potency, which indicates the concentration of the drug needed to inhibit biological activity of a protein by half (i.e., 50%). The MSM simulations are able to distinguish the binding affinities of the ligand molecules that are structurally similar to each other, and the stationary probabilities so obtained correlate quite well with the experimental results. The IC_{50} and stationary probability values are listed in the Table S3 (Supporting Information). The determination of stationary probabilities and the IC_{50} values were performed as a blind test in the sense that the IC_{50} values were not shared with the researcher doing the MSM simulations until the entire analysis was complete. The potency of COB-187 as a selective and reversible inhibitor of GSK-3 α and GSK-3 β has been demonstrated in previous experiments, ^{28,38} which is confirmed by these MSM results.

The ligands in this study are close in the chemical space. For instance, COB-187, COB-152, and COB-180 differ only in the location of the nitrogen atom of the pyridine group. COB-136 and COB-187 differ by a single substitution: in COB-136, the nitrogen in the pyridine ring is replaced by a carbon atom, which dramatically impairs the inhibitory activity of COB-136

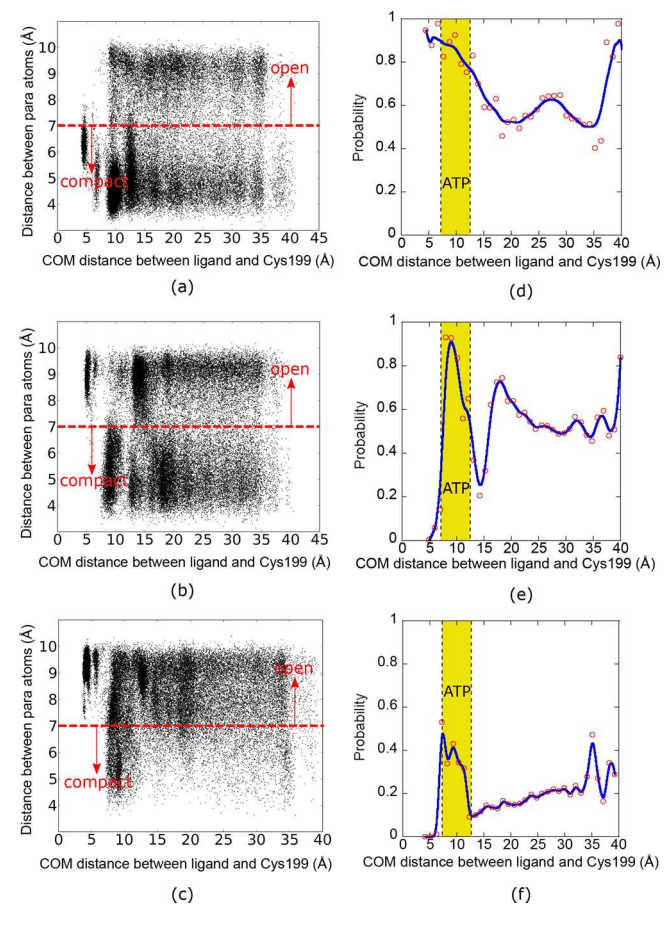


Figure 5. Distribution of the distance between the para atoms of the two six-member aromatic rings as a function of the distance of the ligand from the Cys199 residue in the ATP binding site for (a) COB-187, (b) COB-152, and (c) COB-136 is shown. Ligands are considered in their compact conformation when the distance between the two para atoms is less than 7 Å. The normalized probability distribution of compact conformations as a function of the distance between the ligand molecule and Cys199 for (d) COB-187, (e) COB-152, and (f) COB-136 is also shown. The red points are the probabilities, and the blue line is a smooth fitting line as a guide to the eye. The probability of ligands to attain compact conformations increases when they are within 7–14 Å from Cys199 (yellow band).

versus COB-187. Interestingly, the experimental and MSM results are nicely correlated and suggest a trend wherein the presence of a pyridine and a phenyl ring causes stronger binding to the ATP-binding site of GSK-3 β .

To understand the molecular basis of the differences in the binding affinities of the ligands, we examine the equilibrium conformations of the ligands in the aqueous environment. Figure 3 shows probability distributions of the distance between the atoms at the para position of the two six member ring structures of COB-187, COB-152, COB-180, and COB-136. The para position is the fourth atom in the ring counting from the carbon that is attached to the rest of the molecule. It is observed that the molecules with the pyridine ring display a bimodal probability distribution. The peak in the distribution at smaller distances in Figure 3 corresponds to the stacking of the pyridine and the phenyl groups. Due to the absence of the pyridine group in COB-136, its distribution is broad but unimodal with the peak at the shorter distance absent. The effect of the pyridine group is more pronounced for COB-187 where the nitrogen is in the para position. Changing the

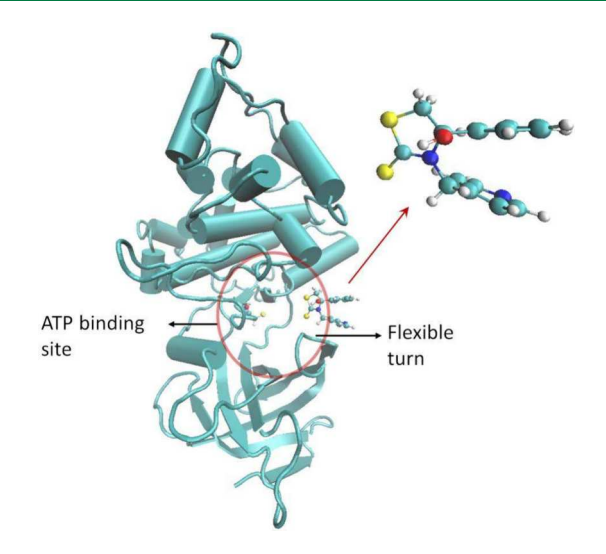


Figure 6. Snapshot of the simulation in which COB-187 is entering the ATP binding site. A turn comprising residues Ile-62 to Gly-68 and a helix (Val-139 to Tyr-150) forms a narrow gap to the ATP-binding site. COB-187 is seen in its compact conformation in the snapshot.

position of the nitrogen atom from the para position in COB-187 to the meta position in COB-152 results in a reduced probability of the first peak, that is, its compact conformation. When the position is changed to ortho (COB-180), the first peak is further reduced. In the Amber ff14SB force field, the Lennard-Jones well depth of nitrogen atom is 0.17 kcal/mol whereas for sp2 carbon, it is 0.086 kcal/mol. Therefore, the nitrogen atom has a stronger affinity for the sp2 carbon atoms of the phenyl ring, which results in the propensity of the ligands with a pyridine ring to attain a compact conformation. When nitrogen is at the para position, the torque from nitrogen-carbon interactions (with the 5-member ring as the fulcrum) is stronger as compared to when the nitrogen is in the meta and ortho positions. This is because when the nitrogen atom is at the para position, the fulcrum associated with the compact conformation is the farthest from the nitrogen atom. From these results, we hypothesize that to access the ATP binding site the molecules need to achieve a compact conformation wherein the two ring structures are stacked together.

We perform funnel metadynamics to simulate numerous binding and unbinding events to test if indeed the compact conformation of the ligands facilitates their binding to the ATP binding site of GSK-3 β . In this methodology, the ligand molecule is restricted to be within a funnel-shaped region (Figure 4). The mouth of the funnel encompasses the ATP binding site, which allows sufficient configurational freedom to the ligand to bind in its favored configuration. The stem of the funnel restricts the region that the ligand samples away from the protein. Through well-tempered metadynamics, we sample multiple binding-unbinding events of the ligands. In the well-tempered metadynamics, the initial Gaussian height of 1.2 kJ/mol and a Gaussian width of 0.15 nm is chosen. The bias factor is set to 8, and the temperature is 310 K. We use the same funnel geometry for all the ligands studied (Figure 4(b)).

Figure 5a—c shows the distribution of the distance between the para atoms of the two six-member aromatic groups of the ligand molecules as a function of the center-of-mass distance of the ligand molecule from Cys199 (a representative residue in the ATP binding site) for COB-187, COB-152, and COB-136

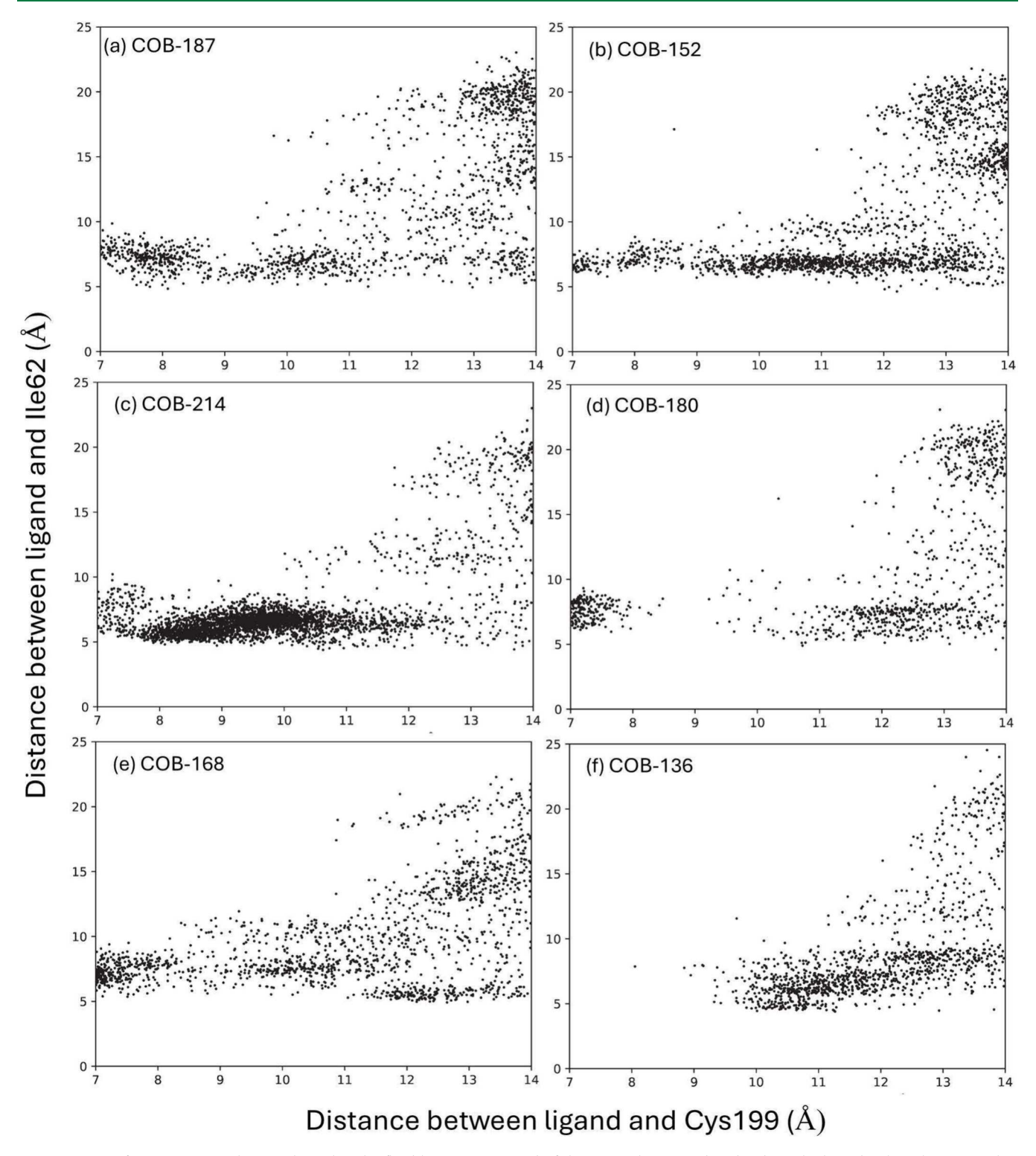


Figure 7. Data from MSM simulations show that the flexible turn composed of Ile-62 to Gly-68 residues binds to the ligands when they are within 7-11 Å from the Cys-199 residue of the ATP-binding site.

respectively. From Figure 3, one can deduce that when the distance between the two para atoms is less than 7 Å, the ligands are in their compact conformation and when it is above 7 Å, they are in the open conformation. Figure 5d—f shows the probability of the compact conformation as a function of the distance of the ligand from Cys199. We find that when the ligand is 7 to 14 Å from Cys199, the probability of the compact conformation increases. COB-187 has the highest probability

of being in the compact form followed by COB-152 and COB-136. This suggests that, to bind to the ATP-binding site, the ligands need to attain the compact conformation.

Figure 6 shows a snapshot of a COB-187 molecule entering the ATP-binding site. A flexible turn comprising of the residues Ile-62 to Gly-68 and a helix (Val-139 to Tyr-150) forms a narrow gap to the binding site. The figure also shows that COB-187 is in its compact conformation, which likely helps it

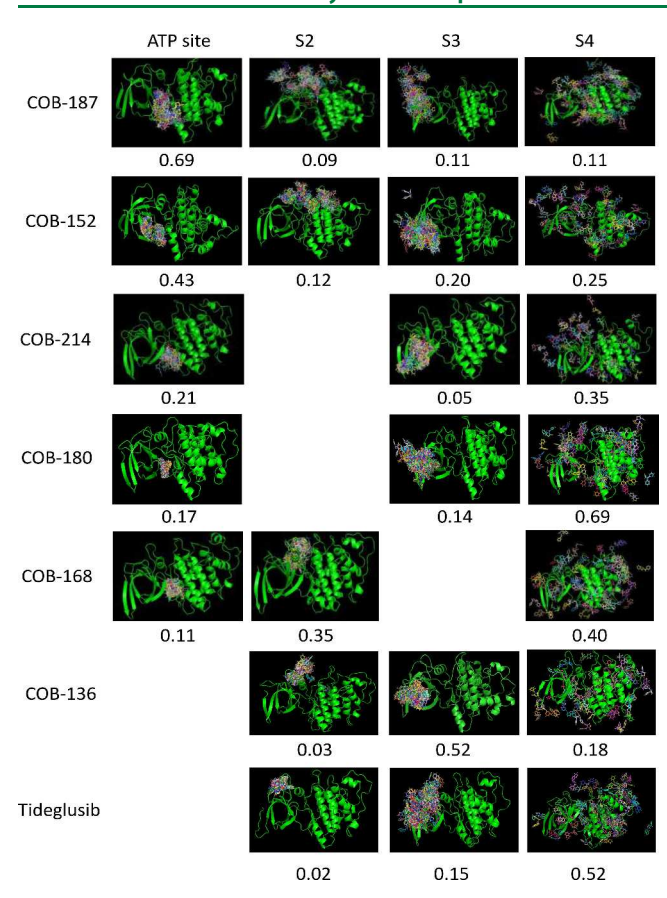


Figure 8. Different macrostates identified by the MSM analysis. Each column represents a specific binding site. Some panels are missing because the corresponding binding sites are not found in the MSM. The number below each macrostate is its stationary probability.

in crossing this gap. Further analysis of the MD trajectories reveals that the flexible turn comprising of mainly hydrophobic residues, Ile-62, Gly-63, Asn-64, Gly-65, Ser-66, Phen-67, and Gly-68, remains bound to the ligands when the ligands are close to the ATP-binding site. This is illustrated in Figure 7 where we have plotted data from our MSM trajectories. The figure shows that when the ligands are within 7 to 11 Å from Cys199, the Ile-62 residue remains close to the ligands. We do not understand as yet if the binding of the turn to the ligands promotes or inhibits the binding of the ligands to the ATP-binding site.

Figure 8 shows snapshots of different ligand-bound and unbound macrostates identified in the MSM of the ligands. It should be noted that the MD simulations only have a single ligand molecule in the simulation box. The snapshots are collections of many configurations. The stationary probability of each macrostate found in the MSM analysis is also listed in the figure. As discussed, COB-187 is the strongest binder to the ATP binding site followed by COB-152. Table S2 (Supporting Information) lists the amino acids associated with the different binding sites on GSK-3 β . The S2 binding site for COB-187, COB-152, and COB-168 matches with the substrate binding site reported for GSK-3\(\beta\). So In contrast to COB-187 and COB-152, COB-168 shows weak binding to the ATP binding site but a stronger affinity for the substrate binding site. Interestingly, COB-136 has strong affinity for an off-target binding site on GSK-3 β located in the β -sheet region close to the N-terminus rather than for the ATP or the

substrate binding site. The ATP-binding, substrate-binding, and S3-binding sites found in the MSM were also identified previously using the mixed solvent MD approach.⁵⁷ MSM estimates the transition rates or flux between the different macrostates. These transition rate maps are shown in Figure S11 (Supporting Information).

4. CONCLUSIONS

Our experimental studies of inhibition of GSK-3 β activity by ligands show that single-atom modifications in the ligands' chemical structure significantly alter their inhibition efficacy. The binding propensity of these ligands on the ATP binding site of GSK-3 β , obtained from Markov State modeling performed on fully atomistic simulations, match quite well with the IC₅₀ values obtained in the experiments. The simulations reveal that the propensity of the ligands to attain a compact conformation helps them to strongly bind to the ATP binding site. The presence of a nitrogen atom in an aromatic ring of the ligand facilitates the attainment of the compact ligand conformations. Protein-ligand binding is understood to be influenced by numerous factors, including hydrophobic/philic character, size and shape of the binding pockets, the energetics of protein-ligand interactions, conformational dynamics of the protein, accessibility to the binding pocket, and entropic factors like the release of bound water and loss of conformational entropy of the ligands and protein residues upon binding. This work reveals that small changes in the chemical structure of the ligands can alter their conformational distribution, which can also significantly influence their binding propensity. In this work, we are studying ligands that are chemically similar to each other and are binding to the same binding site of the protein. So, other factors that may influence the binding propensity are also similar for these ligands. The differences in the conformational diversity of these ligands becomes the dominant factor in deciding their binding propensity. While the results presented in this work are specific to GSK-3 β , one would anticipate the conformational distribution of ligands to be an important factor in other protein-ligand systems as well. Even though many kinases in humans are structurally similar to GSK-3 β , COB-187 is selective for GSK-3 β . It will be interesting to examine if the correlation between the binding propensity and the conformational distribution of ligands is the reason for this selectivity.

ASSOCIATED CONTENT

Supporting Information

The Supporting Information is available free of charge at https://pubs.acs.org/doi/10.1021/acs.jctc.4c00311.

MSM parameters for different ligands; details of the bound states of the ligands; ATP binding stationary probability and IC_{50} values of the ligands; VAMP2 scores for the MSM of COB-187; implied time scale plots of the ligands; probability distributions of the distance between the para atoms of the two sixmembered aromatic rings of different ligands; Chapman-Kolmogorov tests of the ligands; MSM transition rate maps between the microstates for the ligands (PDF)

AUTHOR INFORMATION

Corresponding Author

Sumit Sharma — Department of Chemical and Biomolecular Engineering, Ohio University, Athens, Ohio 45701, United States; orcid.org/0000-0003-3138-5487; Email: sharmas@ohio.edu

Authors

Ramin Mehrani – Department of Mechanical Engineering, Ohio University, Athens, Ohio 45701, United States

Jagannath Mondal — Center for Interdisciplinary Sciences, Tata Institute of Fundamental Research, Hyderabad 500046, India; ⊚ orcid.org/0000-0003-1090-5199

Davoud Ghazanfari — Department of Chemical and Biomolecular Engineering, Ohio University, Athens, Ohio 45701, United States

Douglas J. Goetz – Department of Chemical and Biomolecular Engineering and Biomedical Engineering Program, Ohio University, Athens, Ohio 45701, United States

Kelly D. McCall — Biomedical Engineering Program, Department of Specialty Medicine, The Diabetes Institute, Molecular and Cellular Biology Program, and Translational Biomedical Sciences Program, Ohio University, Athens, Ohio 45701, United States

Stephen C. Bergmeier — Department of Chemistry and Biochemistry and Biomedical Engineering Program, Ohio University, Athens, Ohio 45701, United States; orcid.org/0000-0003-3891-8442

Complete contact information is available at: https://pubs.acs.org/10.1021/acs.jctc.4c00311

Notes

Ohio University owns patents related to COB-187. S.C.B., K.D.M., and D.J.G. are inventors on the patents. The authors declare no competing financial interest.

ACKNOWLEDGMENTS

This work is supported by the NSF CDS&E Grant 1953311 and National Institutes of Health Grant R15GM110602. Computational resources for this work were provided by the National Science Foundation ACCESS Grant Number DMR190005. The authors thank Ohio University Supercomputing Funds for supporting the use of the Ohio Supercomputer Center. The authors acknowledge Mr. Ramtin Mehrani for performing the analysis presented in Figure 7.

REFERENCES

- (1) Sadybekov, A. V.; Katritch, V. Computational approaches streamlining drug discovery. *Nature* **2023**, *616*, 673–685.
- (2) Bowman, G. R.; Pande, V. S.; Noé, F. An introduction to Markov state models and their application to long timescale molecular simulation; Springer Science & Business Media, 2013; Vol. 797.
- (3) Chodera, J. D.; Noé, F. Markov state models of biomolecular conformational dynamics. *Curr. Opin. Struct. Biol.* **2014**, 25, 135–144.
- (4) Husic, B. E.; Pande, V. S. Markov state models: From an art to a science. *J. Am. Chem. Soc.* **2018**, *140*, 2386–2396.
- (5) Shukla, D.; Hernández, C. X.; Weber, J. K.; Pande, V. S. Markov state models provide insights into dynamic modulation of protein function. *Accounts of chemical research* **2015**, *48*, 414–422.
- (6) Linker, S. M.; Magarkar, A.; Köfinger, J.; Hummer, G.; Seeliger, D. Fragment binding pose predictions using unbiased simulations and Markov-state models. *J. Chem. Theory Comput.* **2019**, *15*, 4974–4981.

- (7) Gu, S.; Silva, D.-A.; Meng, L.; Yue, A.; Huang, X. Quantitatively characterizing the ligand binding mechanisms of choline binding protein using Markov state model analysis. *PLoS computational biology* **2014**, *10*, e1003767.
- (8) Thayer, K. M.; Lakhani, B.; Beveridge, D. L. Molecular dynamics—Markov state model of protein ligand binding and Allostery in CRIB-PDZ: conformational selection and induced fit. *J. Phys. Chem. B* **2017**, *121*, 5509—5514.
- (9) Takahashi, R.; Gil, V. A.; Guallar, V. Monte Carlo free ligand diffusion with Markov state model analysis and absolute binding free energy calculations. *J. Chem. Theory Comput.* **2014**, *10*, 282–288.
- (10) Plattner, N.; Noé, F. Protein conformational plasticity and complex ligand-binding kinetics explored by atomistic simulations and Markov models. *Nat. Commun.* **2015**, *6*, 7653.
- (11) Hata, H.; Tran, D. P.; Sobeh, M. M.; Kitao, A. Binding free energy of protein/ligand complexes calculated using dissociation Parallel Cascade Selection Molecular Dynamics and Markov state model. *Biophysics and Physicobiology* **2021**, *18*, 305–316.
- (12) Bernetti, M.; Masetti, M.; Recanatini, M.; Amaro, R. E.; Cavalli, A. An integrated Markov state model and path metadynamics approach to characterize drug binding processes. *J. Chem. Theory Comput.* **2019**, *15*, 5689–5702.
- (13) Dandekar, B. R.; Mondal, J. Capturing protein-ligand recognition pathways in coarse-grained simulation. *J. Phys. Chem. Lett.* **2020**, *11*, 5302-5311.
- (14) Guo, Y.; Duan, M.; Yang, M. The observation of ligand-binding-relevant open states of fatty acid binding protein by molecular dynamics simulations and a Markov state model. *International journal of molecular sciences* **2019**, *20*, 3476.
- (15) Wang, L.; Berne, B.; Friesner, R. Ligand binding to protein-binding pockets with wet and dry regions. *Proc. Natl. Acad. Sci. U. S. A.* **2011**, *108*, 1326–1330.
- (16) Setny, P.; Baron, R.; McCammon, J. A. How can hydrophobic association be enthalpy driven? *J. Chem. Theory Comput.* **2010**, *6*, 2866–2871.
- (17) Cline, G. W.; Johnson, K.; Regittnig, W.; Perret, P.; Tozzo, E.; Xiao, L.; Damico, C.; Shulman, G. I. Effects of a novel glycogen synthase kinase-3 inhibitor on insulin-stimulated glucose metabolism in Zucker diabetic fatty (fa/fa) rats. *Diabetes* **2002**, *51*, 2903–2910.
- (18) Patel, S.; Doble, B. W.; MacAulay, K.; Sinclair, E. M.; Drucker, D. J.; Woodgett, J. R. Tissue-specific role of glycogen synthase kinase 3β in glucose homeostasis and insulin action. *Molecular and cellular biology* **2008**, 28, 6314–6328.
- (19) McCubrey, J. A.; Steelman, L.; Bertrand, F. E.; Davis, N. M.; Abrams, S. L.; Montalto, G.; D'Assoro, A. B.; Libra, M.; Nicoletti, F.; Maestro, R.; et al. others Multifaceted roles of GSK-3 and Wnt/ β -catenin in hematopoiesis and leukemogenesis: opportunities for therapeutic intervention. *Leukemia* **2014**, *28*, 15–33.
- (20) McCubrey, J. A.; Rakus, D.; Gizak, A.; Steelman, L. S.; Abrams, S. L.; Lertpiriyapong, K.; Fitzgerald, T. L.; Yang, L. V.; Montalto, G.; Cervello, M.; et al. Effects of mutations in Wnt/ β -catenin, hedgehog, Notch and PI3K pathways on GSK-3 activity—Diverse effects on cell growth, metabolism and cancer. *Biochimica et Biophysica Acta* **2016**, 1863, 2942–2976.
- (21) Woodgett, J. R. Molecular cloning and expression of glycogen synthase kinase-3/factor A. *EMBO journal* **1990**, *9*, 2431–2438.
- (22) Embi, N.; Rylatt, D. B.; Cohen, P. Glycogen synthase kinase-3 from rabbit skeletal muscle: Separation from cyclic-AMP-dependent protein kinase and phosphorylase kinase. *European Journal of biochemistry* **1980**, *107*, 519–527.
- (23) Cormier, K. W.; Woodgett, J. R. Recent advances in understanding the cellular roles of GSK-3. F1000Research 2017, 6, 167.
- (24) Hanger, D. P.; Hughes, K.; Woodgett, J. R.; Brion, J.-P.; Anderton, B. H. Glycogen synthase kinase-3 induces Alzheimer's disease-like phosphorylation of tau: generation of paired helical filament epitopes and neuronal localisation of the kinase. *Neuroscience letters* 1992, 147, 58–62.

- (25) Mandelkow, E.-M.; Drewes, G.; Biernat, J.; Gustke, N.; Van Lint, J.; Vandenheede, J. v.; Mandelkow, E. Glycogen synthase kinase-3 and the Alzheimer-like state of microtubule-associated protein tau. *FEBS letters* **1992**, 314, 315–321.
- (26) Beurel, E.; Grieco, S. F.; Jope, R. S. Glycogen synthase kinase-3 (GSK3): regulation, actions, and diseases. *Pharmacology & therapeutics* **2015**, *148*, 114–131.
- (27) Lo Monte, F.; Kramer, T.; Gu, J.; Brodrecht, M.; Pilakowski, J.; Fuertes, A.; Dominguez, J. M.; Plotkin, B.; Eldar-Finkelman, H.; Schmidt, B. Structure-based optimization of oxadiazole-based GSK-3 inhibitors. *European journal of medicinal chemistry* **2013**, *61*, 26–40.
- (28) Noori, M. S.; Bhatt, P. M.; Courreges, M. C.; Ghazanfari, D.; Cuckler, C.; Orac, C. M.; McMills, M. C.; Schwartz, F. L.; Deosarkar, S. P.; Bergmeier, S. C.; et al. others Identification of a novel selective and potent inhibitor of glycogen synthase kinase-3. *American Journal of Physiology-Cell Physiology* **2019**, 317, C1289—C1303.
- (29) Eldar-Finkelman, H.; Martinez, A. GSK-3 inhibitors: preclinical and clinical focus on CNS. Frontiers in molecular neuroscience 2011, 4, 32.
- (30) Arciniegas Ruiz, S. M.; Eldar-Finkelman, H. Glycogen synthase kinase-3 inhibitors: preclinical and clinical focus on CNS-A decade onward. *Frontiers in molecular neuroscience* **2022**, *14*, 792364.
- (31) Stambolic, V.; Ruel, L.; Woodgett, J. R. Lithium inhibits glycogen synthase kinase-3 activity and mimics wingless signalling in intact cells. *Current biology* **1996**, *6*, 1664–1669.
- (32) Domínguez, J. M.; Fuertes, A.; Orozco, L.; del Monte-Millán, M.; Delgado, E.; Medina, M. Evidence for irreversible inhibition of glycogen synthase kinase- 3β by tideglusib. *J. Biol. Chem.* **2012**, 287, 893–904.
- (33) Martinez, A.; Alonso, M.; Castro, A.; Dorronsoro, I.; Gelpí, J. L.; Luque, F. J.; Pérez, C.; Moreno, F. J. SAR and 3D-QSAR studies on thiadiazolidinone derivatives: exploration of structural requirements for glycogen synthase kinase 3 inhibitors. *Journal of medicinal chemistry* **2005**, 48, 7103–7112.
- (34) Lovestone, S.; Boada, M.; Dubois, B.; Hüll, M.; Rinne, J. O.; Huppertz, H.-J.; Calero, M.; Andres, M. V.; Gomez-Carrillo, B.; Leon, T.; et al. others A phase II trial of tideglusib in Alzheimer's disease. *Journal of Alzheimer's Disease* **2015**, *45*, 75–88.
- (35) Bhat, R.; Xue, Y.; Berg, S.; Hellberg, S.; Ormö, M.; Nilsson, Y.; Radesäter, A.-C.; Jerning, E.; Markgren, P.-O.; Borgegård, T.; et al. others Structural insights and biological effects of glycogen synthase kinase 3-specific inhibitor AR-A014418. *J. Biol. Chem.* **2003**, 278, 45937–45945.
- (36) Anraku, T.; Kuroki, H.; Kazama, A.; Bilim, V.; Tasaki, M.; Schmitt, D.; Mazar, A.; Giles, F. J.; Ugolkov, A.; Tomita, Y. Clinically relevant GSK-3 β inhibitor 9-ING-41 is active as a single agent and in combination with other antitumor therapies in human renal cancer. *International journal of molecular medicine* **2019**, 45, 315–323.
- (37) Kuroki, H.; Anraku, T.; Kazama, A.; Bilim, V.; Tasaki, M.; Schmitt, D.; Mazar, A. P.; Giles, F. J.; Ugolkov, A.; Tomita, Y. 9-ING-41, a small molecule inhibitor of GSK-3beta, potentiates the effects of anticancer therapeutics in bladder cancer. *Sci. Rep.* **2019**, *9*, 1–9.
- (38) Ghazanfari, D.; Noori, M. S.; Bergmeier, S. C.; Hines, J. V.; McCall, K. D.; Goetz, D. J. A novel GSK-3 inhibitor binds to GSK-3 β via a reversible, time and Cys-199-dependent mechanism. *Bioorg. Med. Chem.* **2021**, *40*, 116179.
- (39) Martin, M.; Rehani, K.; Jope, R. S.; Michalek, S. M. Toll-like receptor—mediated cytokine production is differentially regulated by glycogen synthase kinase 3. *Nature immunology* **2005**, *6*, 777—784.
- (40) Coperchini, F.; Chiovato, L.; Rotondi, M. Interleukin-6, CXCL10 and infiltrating macrophages in COVID-19-related cytokine storm: not one for all but all for one! *Frontiers in immunology* **2021**, 12, 668507.
- (41) Noori, M. S.; Courreges, M. C.; Bergmeier, S. C.; McCall, K. D.; Goetz, D. J. Modulation of LPS-induced inflammatory cytokine production by a novel glycogen synthase kinase-3 inhibitor. *European journal of pharmacology* **2020**, *883*, 173340.
- (42) Ghazanfari, D.; Courreges, M. C.; Belinski, L.; Bergmeier, S. C.; McCall, K. D.; Goetz, D. J. Evidence for investigating GSK-3

- inhibitors as potential therapeutics for severe COVID-19. *Biochem. Biophys. Res. Commun.* **2022**, *605*, 171–176.
- (43) Ghazanfari, D.; Courreges, M. C.; Belinski, L. E.; Hogrell, M. J.; Lloyd, J.; C. Bergmeier, S.; McCall, K. D.; Goetz, D. J. Mechanistic insights into SARS-CoV-2 spike protein induction of the chemokine CXCL10. *Sci. Rep.* **2024**, *14*, 11179.
- (44) Fiser, A.; Šali, A. Methods in enzymology; Elsevier, 2003; Vol. 374, pp 461–491.
- (45) Jorgensen, W. L.; Chandrasekhar, J.; Madura, J. D.; Impey, R. W.; Klein, M. L. Comparison of simple potential functions for simulating liquid water. *J. Chem. Phys.* **1983**, *79*, 926–935.
- (46) Case, D. A.; Cheatham, T. E., III; Darden, T.; Gohlke, H.; Luo, R.; Merz, K. M., Jr; Onufriev, A.; Simmerling, C.; Wang, B.; Woods, R. J. The Amber biomolecular simulation programs. *Journal of computational chemistry* **2005**, *26*, 1668–1688.
- (47) Salomon-Ferrer, R.; Case, D. A.; Walker, R. C. An overview of the Amber biomolecular simulation package. *Wiley Interdisciplinary Reviews: Computational Molecular Science* **2013**, *3*, 198–210.
- (48) Maier, J. A.; Martinez, C.; Kasavajhala, K.; Wickstrom, L.; Hauser, K. E.; Simmerling, C. ff14SB: improving the accuracy of protein side chain and backbone parameters from ff99SB. *J. Chem. Theory Comput.* **2015**, *11*, 3696–3713.
- (49) Pérez-Hernández, G.; Paul, F.; Giorgino, T.; De Fabritiis, G.; Noé, F. Identification of slow molecular order parameters for Markov model construction. *J. Chem. Phys.* **2013**, *139*, No. 07B604 1.
- (50) Schwantes, C. R.; Pande, V. S. Improvements in Markov state model construction reveal many non-native interactions in the folding of NTL9. *J. Chem. Theory Comput.* **2013**, *9*, 2000–2009.
- (51) Naritomi, Y.; Fuchigami, S. Slow dynamics in protein fluctuations revealed by time-structure based independent component analysis: the case of domain motions. *J. Chem. Phys.* **2011**, *134*, No. 02B617.
- (52) Naritomi, Y.; Fuchigami, S. Slow dynamics of a protein backbone in molecular dynamics simulation revealed by time-structure based independent component analysis. *J. Chem. Phys.* **2013**, *139*, 12B605_1.
- (53) Röblitz, S.; Weber, M. Fuzzy spectral clustering by PCCA+: application to Markov state models and data classification. *Advances in Data Analysis and Classification* **2013**, *7*, 147–179.
- (54) Prinz, J.-H.; Wu, H.; Sarich, M.; Keller, B.; Senne, M.; Held, M.; Chodera, J. D.; Schütte, C.; Noé, F. Markov models of molecular kinetics: Generation and validation. *J. Chem. Phys.* **2011**, *134*, 174105.
- (55) Scherer, M. K.; Trendelkamp-Schroer, B.; Paul, F.; Pérez-Hernández, G.; Hoffmann, M.; Plattner, N.; Wehmeyer, C.; Prinz, J.-H.; Noé, F. PyEMMA 2: A Software Package for Estimation, Validation, and Analysis of Markov Models. *J. Chem. Theory Comput.* **2015**, *11*, 5525–5542.
- (56) Cohen, P.; Frame, S. The renaissance of GSK3. *Nat. Rev. Mol. Cell Biol.* **2001**, 2, 769–776.
- (57) DasGupta, D.; Mehrani, R.; Carlson, H. A.; Sharma, S. Identifying Potential Ligand Binding Sites on Glycogen Synthase Kinase 3 Using Atomistic Cosolvent Simulations. ACS Applied Bio Materials 2024, 7, 588–595.